Journal of Materials Chemistry C

PAPER

Check for updates

Cite this: J. Mater. Chem. C, 2017, 5, 3830

A tunable and sizable bandgap of a g-C_3N_4/graphene/g-C_3N_4 sandwich heterostructure: a van der Waals density functional study

M. M. Dong, [a] C. He *[a] and W. X. Zhang*[b]

Received 23rd January 2017,
Accepted 20th March 2017

DOI: 10.1039/c7tc00386b

rsc.li/materials-c

The structural and electronic properties of a g-C_3N_4/graphene/g-C_3N_4 (g-C_3N_4/SLG/g-C_3N_4) sandwich heterostructure have been systematically investigated using density functional theory with van der Waals corrections. The results indicate that the band gap of the g-C_3N_4/SLG/g-C_3N_4 sandwich heterostructure can be opened to 106 meV without strain. Applying strain is a promising way to tune the electronic properties of a sandwich heterostructure. After applying uniaxial strain, the heterostructure can withstand larger tensile strain than compression strain without damaging the structure and the band gap is more easily increased by the *X*-direction strain. When the 5% *X*-direction strain is applied, the band gap could be opened to 525 meV and meanwhile maintain a high carrier mobility. These electronic properties may provide a potential application in nanodevices.

Introduction

Two-dimensional (2D) materials are expected to replace traditional semiconductor silicon materials and have attracted great attention,[1–4] due to their excellent properties and potential applications in nanoelectronics and spintronics. Since graphene was fabricated by Novoselov *et al.* as a transferable material in 2004,[5] it has been a hot research topic because of its excellent electron mobility, high thermal conductivity, great mechanical properties and stability.[6,7] However, the lack of a band gap seriously limits its actual application in graphene-based microelectronic devices with a high on/off ratio and a large switching off current.

In order to open a band gap in graphene, various methods have been proposed, such as cutting graphene into nanoribbons,[8] chemical functionalization,[9] heterostructures[10–12] and application of strain or external electric field.[13,14] These methods depending on whether they preserve the integrity of the honeycomb structure could be classified into two types. When the honeycomb structure is destroyed, the carrier mobility and the on/off ratio are greatly reduced. Because the destruction of the honeycomb structure introduces scattering centers, enhances the carrier effective mass and produces a non-tunable band gap.[15] When the honeycomb structure is preserved as a heterostructure by applying strain or an external electric field a high carrier mobility could be maintained exhibiting a tunable band gap. Among these approaches, heterostructures provide an optimal way for tuning the electronic properties of graphene. The common substrates for graphene FETs include SiO_2,[16] BN,[17] MoS_2[11,18] and phosphorene.[10,12] Despite these achievements, the search for ideal substrates is still underway.

C_3N_4, a novel non-metallic material, which responds to visible light, has several allotropes, namely the α-phase, the β-phase, the cubic phase, the quasi-cubic phase and the graphitic carbon nitride phase (g-C_3N_4). g-C_3N_4 (the band gap is 2.7 eV for bulk materials) is considered to be the most stable one under ambient conditions.[19] Very recently, with the advantages of non-toxic, a visible light response, easy for preparation, in addition to its photocatalytic aspects, g-C_3N_4 has attracted great attention because of its conceivable application in electronic devices.[20–23] Previous research shows that the band gap of the graphene/g-C_3N_4 bilayers can be opened up to 108.5 meV, and by applying external electric field the band gap of graphene/g-C_3N_4 bilayers can be tuned effectively.[24] Du *et al.*[20] investigated the interface between optically active graphitic carbon nitride (g-C_3N_4) and electronically active graphene. They reported that the strong electronic coupling at the graphene/g-C_3N_4 interface opened a 70 meV bandgap in g-C_3N_4-supported graphene. And the hybrid graphene/g-C_3N_4 could obviously expand the absorption and utilization of visible light and exhibit high photocatalytic activity when compared to a pure g-C_3N_4 monolayer. The study reported by Yu *et al.*[23] showed that graphene could be used as an electronically conductive channel to effectively separate photogenerated carriers in graphene/g-C_3N_4 composites, thereby improving the photocatalytic activity of g-C_3N_4. And it is reported that the different stacking models of graphene and g-C_3N_4 can also regulate the

[a] State Key Laboratory for Mechanical Behavior of Materials, School of Materials Science and Engineering, Xi'an Jiaotong University, Xi'an 710049, China. E-mail: hecheng@mail.xjtu.edu.cn
[b] School of Materials Science and Engineering, Chang'an University, Xi'an 710064, China. E-mail: wxzhang@chd.edu.cn

band gap of g-C_3N_4/graphene heterostructures.[24] However, the range of bandgap is relatively small, which still can not meet the business needs. In order to further expand the possible application of g-C_3N_4 in electronic devices, the following studies are necessary.

In addition, studies have shown that the sandwich heterostructures could break the interlayer symmetry.[25,26] By adjusting the spacing of the layers, the dipole moments and shielding charge distributions between the layers could be significantly changed thereby adjusting the band compensation of the heterostructure. The sandwich structures such as h-BN/SLG/h-BN,[26] h-BN/MoS_2/h-BN[27] and graphene/h-BN/GaAs[25] exhibit more excellent performance. It is reported that the h-BN/SLG/h-BN sandwich heterostructure could provide the sensor with a better resistance to corrosion and a transient response. And researchers of the University of Manchester have published that laminating 2D materials into a new material, a SLG/h-BN/SLG sandwich heterostructure, could exhibit excellent capabilities in the future as a preferred material for manufacturing next-generation transistors. Therefore, in this work, g-C_3N_4/SLG/g-C_3N_4 sandwich heterostructures are built by stacking single layer graphene (SLG) in the middle of bilayer g-C_3N_4. First principles calculations with vdW-corrected, exchange–correlation functional are devoted to evaluate the stacking patterns, structure stability and the electronic properties. Then, we tune the electronic properties of the heterostructure by applying biaxial or uniaxial strain. These studies might provide us with a deep understanding of the g-C_3N_4/SLG/g-C_3N_4 system, which is promising for future nanodevices.

Theoretical approach

The first-principles DFT calculations are performed within the DMol^3 code.[28] The generalized gradient approximation (GGA) with the Perdew–Burke–Ernzerhof (PBE)[29] functional is utilized as the exchange–correlation functional. The effect of vdW interactions is taken into account by using the empirical correction scheme proposed by Grimme.[30] It has already been proved that the Grimme method could correctly reproduce the structural properties of the layered materials.[31] And the vdW methods can be improved by the determination of the distance d (interlayer spacing) and give a more accurate description of the dispersion forces between the atomic layers than PBE.[32] Moreover, double numerical atomic orbital plus polarization (DNP) is chosen as the basis set, with a global orbital cutoff of 4.4 Å. The cutoff kinetic energy for plane waves is set to be 450 eV, which is sufficiently large because all the results are converged at this value. The convergence tolerance of energy, maximum force, and maximum displacement were set to 1.0×10^{-5} Ha, 0.001 Ha Å^{-1} and 0.005 Å, respectively (1 Ha = 27.2114 eV). The k-point sampling grid is $11 \times 11 \times 1$ for both structural optimization and electronic structural calculations. In geometric optimization, the positions of all atoms in a supercell are fully relaxed while the shape and the volume of the supercell are fixed. The vacuum spacing between neighboring supercells is set to be 20 Å to avoid artificial interactions. The charge density difference is calculated using the CASTEP code in this work.[33]

Binding energy (E_b) can be used to assess the structural stability of the heterostructure system. The formula for the binding energy is that:

$$E_b = E_{\text{hetrostructure}} - E_{\text{graphene}} - 2 \times E_{\text{g-}C_3N_4} \quad (1)$$

where $E_{\text{heterostructure}}$, E_{graphene} and $E_{\text{g-}C_3N_4}$ are, respectively, the energy of a heterostructure system, graphene and g-C_3N_4 with the same lattice parameters. According to this definition, the negative value of E_b means the stable binding of a heterostructure system, and a more negative value indicates a more energetically favorable heterostructure system.

Results and discussion

As usual, a heterostructure is formed easily when the lattice mismatch is small. The lattice parameters of the pristine graphene and g-C_3N_4 monolayers are 2.46 Å and 7.06 Å, respectively. Hence, being similar to the modeling methods of graphene/g-C_3N_4 bilayer structures, we have imposed a commensurability condition between graphene and bilayer g-C_3N_4, where a 1×1 lateral periodicity of bilayer g-C_3N_4 and a 3×3 lateral periodicity of the graphene are employed, resulting in a mismatch of around 4.3%.[24] A supercell is constructed for the sandwich structure of a single layer graphene that is inserted between two g-C_3N_4 single layers.

In addition, the hybrid functionals, such as HSE,[34] PBE0[35] or B3LYP,[36,37] represent the state-of-the-art approach to accurately describe the electronic structure of periodic systems. The hybrid functional is very time consuming and it would quickly become prohibitively expensive as the system size would grow. Thus, it is considered that DFT-PBE based calculations should be enough as long as all the calculations use the same settings.[38,39] Similar structures have been studied in the MoS_2 and h-BN sandwich structures.[27] For the sake of consistency, the interlayer distance (d) is defined as the shortest distance between the graphene layer and the g-C_3N_4 layer. According to previous studies, we define the same d between graphene and the adjacent g-C_3N_4 single layers in the sandwich structures.[27] The g-C_3N_4/SLG/g-C_3N_4 sandwich structure is characterized by both the stacking sequence of its layers and the positions of the C atoms relative to the bottom and top g-C_3N_4 layers.

According to the position of the g-C_3N_4 bilayers relative to graphene, we have constructed five stacking patterns, as shown in Fig. 1, C atoms of g-C_3N_4 locate in the hexagonal ring center of graphene (labeled as H_C), N atoms of g-C_3N_4 locate in the hexagonal ring center of graphene (labeled as H_N). The stacking model when the two g-C_3N_4 layers locate directly above and below of graphene is labeled as T, labeled as B_N when N atoms of g-C_3N_4 locate in the midpoint of the C–C bond, and labeled as B_C when the C atoms of g-C_3N_4 locate in the midpoint of the C–C bond. The corresponding parameters of the five stacking patterns after geometric optimization are listed in Table 1, where the structure B_N is optimized to H_C and B_C is optimized to H_N due to its instability. Therefore, these two stacking patterns B_N and B_C will not be discussed below.

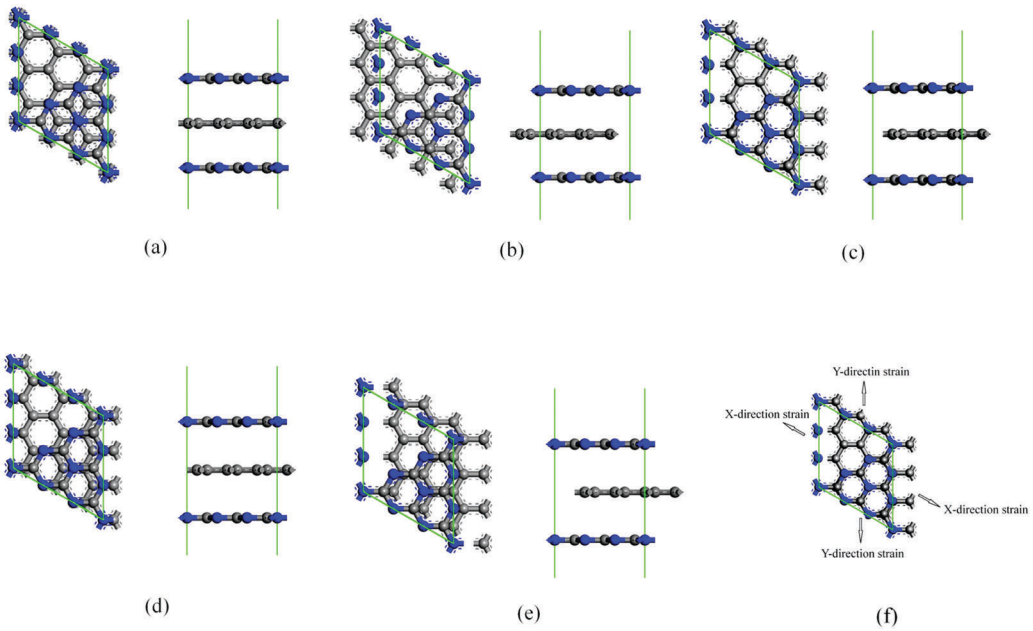

Fig. 1 Side (right) and top (left) views of five atomic configurations for different stacking patterns: (a) H_C, (b) H_N, (c) T, (d) B_N (e) B_C; (f) the schematic diagram of the applied strain for the stacking pattern T g-C_3N_4/graphene/g-C_3N_4 heterostructure.

Table 1 Summary of the structural and electronic properties of different heterostructures. d_0 means the nearest distance between monolayer g-C_3N_4 and the graphene substrates after geometric optimization. The asterisks * are the results after geometric optimization

Type	g-C_3N_4/graphene/g-C_3N_4				
Stacking patterns	H_C	H_N	T	B_N*	B_C*
d_0 (Å)	3.189	3.115	3.286	3.234	3.153
E_b (eV)	−1.5046	−1.67416	−1.35442	−1.8768	−2.1284
E_g (eV)	0.064	0.096	0.106	0.054	0.077
m_e (m_0)	0.06988	0.07439	0.07865	—	—
m_h (m_0)	0.08248	0.07336	0.0852	—	—

Furthermore, we find that the band gap can be increased to a maximum of 0.106 eV by stacking as pattern T. While the band gaps of the three stacking patterns H_C, H_N, T are 0.064 eV, 0.096 eV, 0.106 eV, respectively, and all of them are direct band gaps. It is worth noting that there still exists some discrepancy between the theory and the experiment in predicting numerically accurate values of band gaps for g-C_3N_4 and graphene, partly due to the choices in the exchange–correlation functional, Poisson's ratio[40] and the inclusion of many-body effects. The effective mass of electrons and holes is small and almost the same for these three stacking patterns. Correspondingly, the carrier mobility of heterostructures compared to graphene does not change obviously. Therefore, pattern T has the biggest band gap and the highest binding energy without strain, which should be more easy and effective to open the band gap of graphene among the five stacking modes. Comprehensively considering the band gap, binding energy and effective mass, pattern T of AA stacking should be the best choice among these five stacking patterns to tune the electronic properties of sandwich heterostructures. Hence, we choose pattern T as the object to study the structural and electronic properties of the heterostructure with biaxial or uniaxial strain.

The band structure and the orbital diagram of pattern T are shown in Fig. 2. The pattern T has a direct band gap, where the CBM and the VBM are both located in the Gamma (Γ) point. At the same time, according to the orbital diagram, it can be seen that both the HOMO and the LUMO are located in the graphene monolayer, indicating that the energy band near the Fermi level of the heterostructure is mainly contributed by graphene. The Mulliken charge analysis of the pattern T shows that there is no obvious charge transfer between graphene and g-C_3N_4 layers of the heterostructure, which indicates that the structure mainly interacts with the van der Waals force and that is consistent with the orbital results.

Next we have calculated the relationship between the binding energy, the band gap and the interlayer distance d of pattern T, which is shown in Fig. 3. The diagram can be divided into two parts, according to whether the structure of pattern T can be changed. When d is 3.2–4.5 Å, the structure of pattern T almost does not change. The band gap decreases gradually to 0.006 eV with the increase of d. Because of the calculation error it can be regarded as no band gap when d is up to 4.5 Å. The binding energy is negative and increases gradually in this section, which indicates that the stability of the heterostructure decreases with the increase of d. When d is equal to 3.286 Å, the binding energy has a minimum value (−1.354 eV) and the band gap is 0.106 eV. When d is in the range of 2.0–3.1 Å, the pattern T will spontaneously transform into the H_N pattern, because the repulsive force between graphene and C and N atoms of g-C_3N_4 is enhanced. When d is less than 2.8 Å, the binding energy is positive, which indicates that the heterostructure is unstable. When d is equal to 3.1 Å, the binding energy is the smallest and

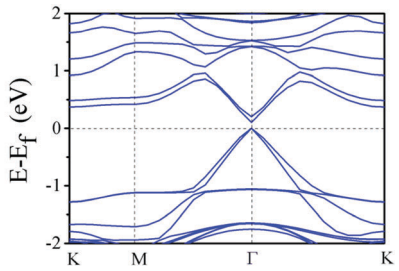

(a) Band structure of the stacking pattern T

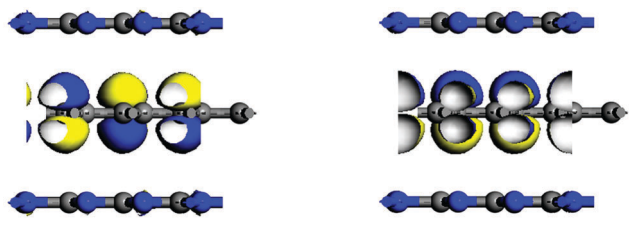

(b) Orbitals of the stacking pattern T

Fig. 2 The band structure and orbitals of the stacking pattern T g-C_3N_4/graphene/g-C_3N_4 sandwich heterostructure.

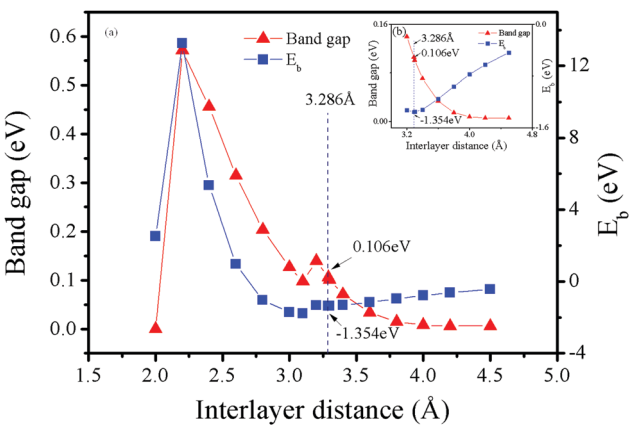

Fig. 3 The binding energy and band gap of the stacking pattern T g-C_3N_4/graphene/g-C_3N_4 heterostructure as a function of interlayer distance d: (a) the general map; (b) the enlarged view for 3.2–4.5 Å.

the band gap is 0.098 eV, which is basically consistent with the result in Table 1 (H_N). Based on the above results, d of the stacking pattern T is preferentially 3.286 Å.

Applying strain has been known as an effective way of controlling the electronic, transport, and optical properties of semiconductors for decades. This is particularly useful for engineering one-dimensional (1D) and two-dimensional (2D) crystals because these reduced-dimensional structures can sustain much larger strains than the corresponding bulk crystals.[41,42]

For clearly understanding the effect of strain on the heterostructure, we have applied a biaxial or uniaxial strain from −12% to +12% on pattern T with d of 3.286 Å as shown in Fig. 4,

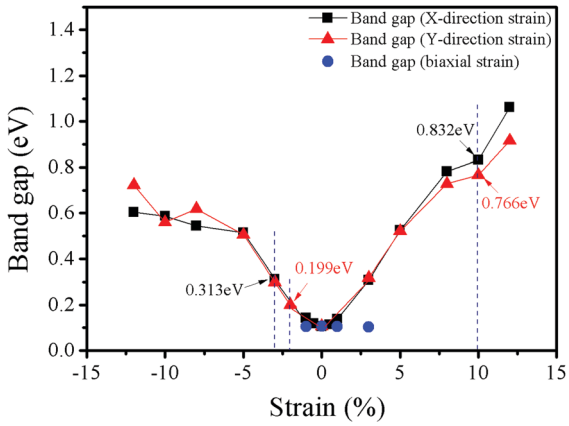

Fig. 4 The band gap of the stacking pattern T g-C_3N_4/graphene/g-C_3N_4 heterostructure as a function of strain.

where we define the tensile strain as positive values, compressive strain as negative values. Positive and negative values represent only the strain type. The uniaxial strains along the X direction and the Y direction have been recorded as the X-direction strain and the Y-direction strain, respectively. The applied direction of the strain is shown in Fig. 1(f), similar methods have also been studied in atomically thin arsenene and antimonene.[43]

We find that the pattern T can only withstand a biaxial strain from −1% to +3% without damaging its structure, and the band gap decreases slightly with the increase of biaxial strain. Therefore, we will only discuss the uniaxial strain below. The structure of pattern T has not obviously changed, when the X-direction strain ranges −3% to +10% and the Y-direction strain ranges −2% to +10%. It indicates that the heterostructure can withstand larger tensile strain. For the X-direction strain when the applied uniaxial strain is greater than +10% or less than −3%, the structure of the T pattern is unstable, moreover, the bilayer g-C_3N_4 will be bent. For the Y-direction strain, there is a similar situation. When the strain is applied, the band gap increases with the increasing strain. For the X-direction strain when applying −3% uniaxial strain, the band gap increases to 0.313 eV, and the band gap increases to 0.832 eV when the uniaxial strain is −10%. For the Y-direction strain when applying −2% uniaxial strain, the band gap increases to 0.199 eV, while the band gap increases to 0.766 eV when the uniaxial strain is −10%. According to the results, we find that without damaging the bond for the structure, the X-direction strain increases the band gap more. This result is consistent with previous study that graphene can withstand more strain distribution parallel to C–C bonds than the strain distribution perpendicular to C–C bonds.[44] The band structure as a function of X-direction strain for the stacking pattern T is shown in Fig. 5, it can be more clearly seen that the bottom of the conduction band shifts up as the strain increases and then the band gap expands. It is also interesting to note that the interlayer spacing d of the heterostructure increases slightly with tensile strain and decreases with the compressive strain. Meanwhile, the change trend of d is consistent with the strain. In addition to opening the band gap for the heterostructure, it is also desirable that the heterostructure

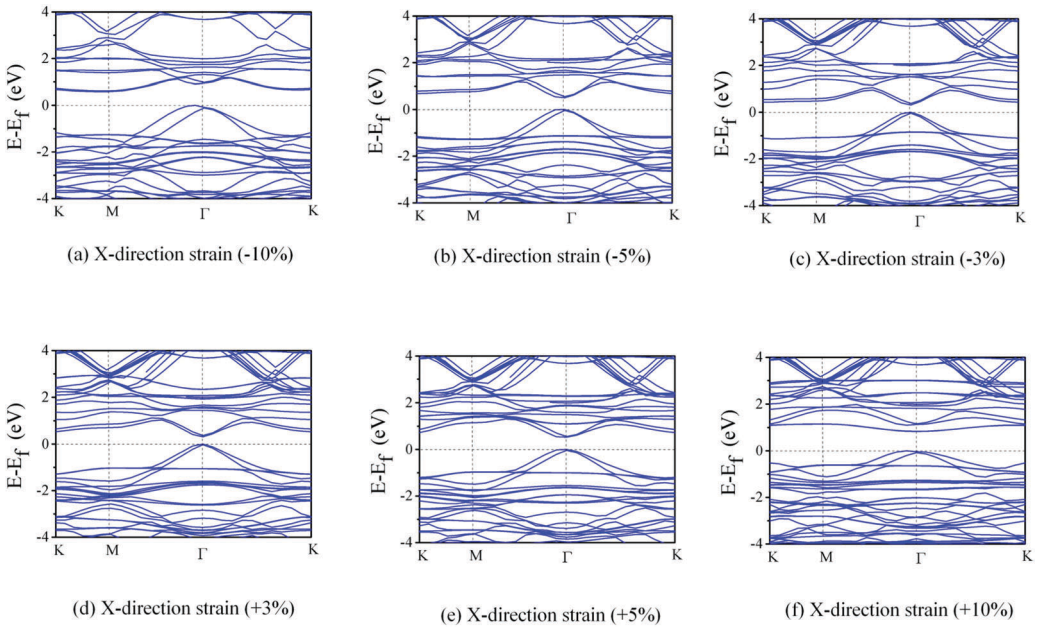

Fig. 5 The band structure of the stacking pattern T g-C_3N_4/graphene/g-C_3N_4 sandwich heterostructure as a function of uniaxial strain.

should be able to maintain its high carrier mobility. Considering the effect of periodic lattices, the smaller the carrier effective mass is, the higher the carrier mobility will be when the other conditions are constant. Therefore, we choose the carrier effective mass as a measurement of the carrier mobility.

The effective mass of the material is closely related to the carrier mobility of the material and the effective mass is calculated according to the following formula:

$$\left(\frac{1}{m^*}\right)_{ij} = \frac{1}{h^2}\frac{\partial^2 E}{\partial k_i \partial k_j}, \quad i,j = x,y,z \tag{2}$$

From eqn (2), we can obtain the effective mass of an electron (or a hole) by the second derivative of the top of the valence band (or the bottom of the conduction band) for the wave vector; although m^* is a second-order tensor with nine components, we can take it as a scalar. Three directions (x, y, z) are calculated when we calculate the energy band.

$$\frac{1}{m^*} = \frac{1}{h^2}\frac{\partial^2 E(k)}{\partial k^2} \tag{3}$$

Therefore, according to the band structure of the g-C_3N_4/SLG/g-C_3N_4 heterostructure in different uniaxial strain strength, we draw the carrier effective mass of the heterostructure with different uniaxial strain intensities, which is shown in Fig. 6. It can be found that the effective mass of electrons and holes of the X-direction strain is almost equal when the strain is −5% to +5%, because the conduction band and the valence band of the heterostructure are almost symmetric at the Dirac point. While for the Y-direction strain, the effective mass of electrons and holes is almost equal when the strain is −8% to +5%. Moreover, we find that the effective mass of the Y-direction strain is larger than the X-direction strain when the pattern T is with the

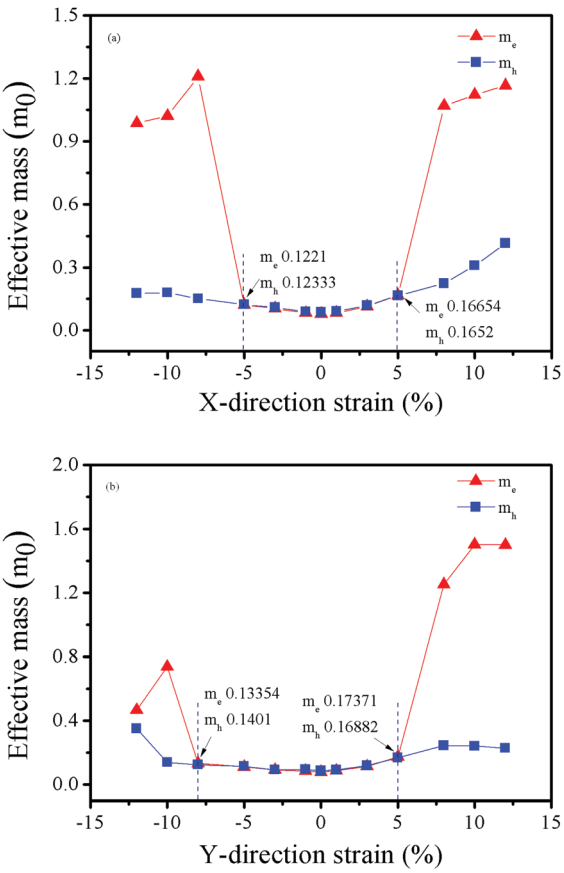

Fig. 6 The variation of the effective mass of the carrier as a function of uniaxial strain for the stacking pattern T g-C_3N_4/graphene/g-C_3N_4 sandwich heterostructure: (a) X-direction strain and (b) Y-direction strain.

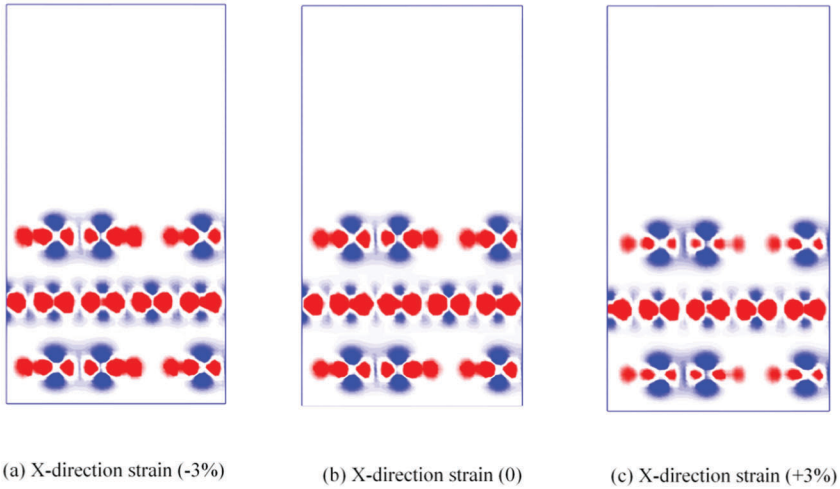

Fig. 7 The charge density difference of the pattern T heterostructure as a function of uniaxial strain: (a) −3% *X*-direction strain, (b) 0 and (c) +3% *X*-direction strain.

same strain. Therefore, the *X*-direction strain is the best choice while taking both the band gap and carrier mobility into account. The effective masses of electrons and holes are $0.07865m_0$ and $0.0852m_0$ without strain. While the effective masses of electrons and holes of graphene/g-C_3N_4 are $0.0183m_0$ and $0.0184m_0$.[24] It can be seen that the effective mass of these two structures is of the same order of magnitude, which means that both of them can maintain a high carrier mobility. The effective mass enhances with the increase of strain, whether negative or positive. It is worth mentioning that when the applied strain is greater than 5%, the electron effective mass increases significantly, the effective mass of the hole rises slowly, so the difference between them increases obviously. It may be due to the destruction of the structure under compressive strain, electrons can easily escape from the conduction band, and then the effective mass of electrons increases significantly. The conductivity pattern of T has transformed from electron–hole to hole by applying tensile strain, and the contribution of electrons as carriers is significantly reduced by the increase of the tensile strain. It can be found that when the 5% *X*-direction strain is applied, the band gap of pattern T can be opened to 0.525 eV and maintain a high carrier mobility.

In order to unravel more information about the bonding mechanism, it is worthwhile to investigate the charge density difference, the results are shown in Fig. 7. According to the red isosurface, it can be seen that under the compressive strain, the atomic distance between the atoms in the same layers of graphene and g-C_3N_4 monolayer is closer, which leads to the enhancement of the interaction among the atoms in the same layers. Hence, the electrons accumulate in the layer of Graphene and g-C_3N_4. The tensile strain increases the distance between the atoms in the same layers, resulting in the weakening of the interaction between the atoms. And the effect of strain on g-C_3N_4 is larger than the graphene monolayer. Correspondingly, as shown by the blue isosurface, the application of compressive strain causes the loss of electrons and tensile strain causes electron accumulation in the interlayer.

Conclusion

In summary, we have investigated the structural and electronic properties of the g-C_3N_4/SLG/g-C_3N_4 sandwich heterostructure using DFT calculations. Five possible stacking patterns have been considered, and the pattern T should be the best choice, since the mobility is not significantly decreased while the band gap is significantly opened to 0.106 eV. Furthermore, the band gap of the pattern T heterostructure can be tuned regularly with an experimentally achievable strain. Meanwhile the carrier effective mass reveals that the g-C_3N_4/SLG/g-C_3N_4 sandwich heterostructure will exhibit a high carrier mobility under appropriate strain. Our results suggest that effectively controlling the stacking patterns and the strain could significantly affect the properties of the heterostructures and open up exciting opportunities for the development of electronic and optoelectronic devices based on the g-C_3N_4/SLG/g-C_3N_4 system.

Acknowledgements

The authors acknowledge support from the National Natural Science Foundation of China (NSFC, Grant No. 51471124 and 51301020), the China Postdoctoral Science Foundation (No. 2015M582585), the special fund for basic scientific research of central colleges of Chang'an University (No. 310831162002) and the Fundamental Research Funds for the Central Universities (No. xjj2016018).

References

1 J. Zhu and U. Schwingenschlogl, Stability and electronic properties of silicene on WSe_2, *J. Mater. Chem. C*, 2015, **3**, 3946–3953.
2 Q. G. Jiang, J. F. Zhang, Z. M. Ao and Y. P. Wu, Density functional theory study on the electronic properties and stability of silicene/silicane nanoribbons, *J. Mater. Chem. C*, 2015, **3**, 3954–3959.

3 N. Gillgren, D. Wickramaratne, Y. Shi, T. Espiritu, J. Yang, J. Hu, J. Wei, X. Liu, Z. Mao, K. Watanabe, T. Taniguchi, M. Bockrath, Y. Barlas, R. K. Lake and C. Ning Lau, Gate Tunable Quantum Oscillations in Air-Stable and High Mobility Few-Layer Phosphorene Heterostructures, *2D Mater.*, 2015, **2**, 011001.

4 Q. G. Jiang, J. F. Zhang, Z. M. Ao and Y. P. Wu, First principles study on the electronic structure and interface stability of hybrid silicene/fluorosilicene Nanoribbons, *Sci. Rep.*, 2015, **5**, 15734–15743.

5 K. S. Novoselov, A. K. Geim, S. Morozov, D. Jiang, Y. Zhang, S. Dubonos, I. Grigorieva and A. A. Firsov, Electricfield effect in atomically thin carbon films, *Science*, 2004, **306**, 666–669.

6 N. Gao, G. Y. Lu, Z. Wen and Q. Jiang, Electronic structure of silicene: effects of the organic molecular adsorption and substrate, *J. Mater. Chem. C*, 2017, **3**, 627–633.

7 C. G. Lee, X. D. Wei, J. W. Kysar and J. Hone, Measurement of the elastic properties and intrinsic strength of monolayer graphene, *Science*, 2008, **321**, 385–388.

8 X. Wang, Y. Ouyang, X. Li, H. Wang, J. Guo and H. Dai, Room-temperature all-semiconducting sub-10-nm graphene nanoribbon field-effect transistors, *Phys. Rev. Lett.*, 2008, **100**, 206803.

9 R. Balog, B. Jorgensen, L. Nilsson, M. Andersen, E. Rienks, M. Bianchi, M. Fanetti, E. Lægsgaard, A. Baraldi, S. Lizzit, Z. Sljivancanin, F. Besenbacher, B. Hammer, T. G. Pedersen, P. Hofmann and L. Hornekær, Bandgap opening in graphene induced by patterned hydrogen adsorption, *Nat. Mater.*, 2010, **9**, 315–319.

10 A. Hashmi, U. Farooq and J. Hong, Graphene/phosphorene bilayer: High electron speed, optical property and semiconductor–metal transition with electric field, *Curr. Appl. Phys.*, 2016, **16**, 318–323.

11 N. Gao, J. C. Li and Q. Jiang, Tunable band gaps in silicene-MoS_2 heterobilayers, *Phys. Chem. Chem. Phys.*, 2014, **16**, 11673–11678.

12 B. Q. You, X. C. Wang, Z. D. Zheng and W. B. Mi, Black phosphorene/monolayer transition-metal dichalcogenides as two dimensional van der Waals heterostructures: a first-principles study, *Phys. Chem. Chem. Phys.*, 2016, **18**, 7381–7388.

13 M. V. Medvedyeva and Y. B. Blanter, Piezoconductivity of gated suspended graphene, *Phys. Rev. B: Condens. Matter Mater. Phys.*, 2011, **83**, 045426.

14 Y. Ma, Y. Dai, M. Guo, C. Niu, Y. Zhu and B. Huang, Evidence of the existence of magnetism in pristine VX_2 monolayers (X = S, Se) and their strain-induced tunable magnetic properties, *ACS Nano*, 2012, **6**, 1695–1701.

15 X. Zhong, R. G. Amorim, R. H. Scheicher, R. Pandey and S. P. Karna, Electronic structure and quantum transport properties of trilayers formed from graphene and boron nitride, *Nanoscale*, 2012, **5**, 5490–5498.

16 N. T. Nguyen, M. Otani and S. Okada, Semiconducting Electronic Property of Graphene Adsorbed on (0001) Surfaces of SiO_2, Boron nitride substrates for high-quality graphene electronics, *Phys. Rev. Lett.*, 2011, **106**, 106801.

17 C. R. Dean, A. F. Young, I. Meric, C. Lee, L. Wang, S. Sorgenfrei, K. Watanabe, T. Taniguchi, P. Kim and K. L. Shepard, Boron nitride substrates for high-quality graphene electronics, *Nat. Nanotechnol.*, 2010, **5**, 722–726.

18 Y. M. Lin, C. Dimitrakopoulos, K. A. Jenkins, D. B. Farmer, H. Y. Chiu, A. Grill and P. Avouris, 100-GHz Transistors from Wafer-Scale Epitaxial Graphene, *Science*, 2010, **327**, 662.

19 S. Martha, A. Nashim and K. Parida, Facile synthesis of highly active g-C_0N_4 for efficient hydrogen production under visible light, *J. Mater. Chem. A*, 2013, **1**, 7816–7824.

20 A. J. Du, S. Sanvito, Z. Li, D. W. Wang, Y. Jiao, T. Liao, Q. Sun, Y. H. Ng, Z. H. Zhu, R. Amal and S. C. Smith, Hybrid Graphene and Graphitic Carbon Nitride Nanocomposite: Gap Opening, Electron-Hole Puddle, Interfacial Charge Transfer, and Enhanced Visible Light Response, *J. Am. Chem. Soc.*, 2012, **134**, 4393–4397.

21 X. J. Wang, C. Liu, X. L. Li, F. T. Li, Y. P. Li, J. Zhao and R. H. Liu, Construction of g-C_3N_4/Al_2O_3 hybrids *viain situ* acidification and exfoliation with enhanced photocatalytic activity, *Appl. Surf. Sci.*, 2016, **394**, 340–350.

22 X. C. Wang, S. Blechert and M. Antonietti, Polymeric Graphitic Carbon Nitride for Heterogeneous Photocatalysis, *ACS Catal.*, 2012, **2**, 1596–1606.

23 Q. J. Xiang, J. G. Yu and M. Jaroniec, Preparation and Enhanced Visible-Light Photocatalytic H_2-Production Activity of Graphene/C_3N_4 Composites, *J. Phys. Chem. C*, 2011, **115**, 7355–7363.

24 X. R. Li, Y. Dai, Y. D. Ma, S. H. Han and B. B. Huang, Graphene/g-C_3N_4 bilayer: considerable band gap opening and effective band structure engineering, *Phys. Chem. Chem. Phys.*, 2014, **16**, 4230–4235.

25 X. Q. Li, S. S. Lin, X. Lin, Z. J. Xu, P. Wang, S. J. Zhang, H. K. Zhong, W. L. Xu, Z. Q. Wu and W. Fang, Graphene/h-BN/GaAs sandwich diode as solar cell and photodetector, *Opt. Express*, 2016, **24**, 134–145.

26 R. Quhe, J. X. Zheng, G. F. Luo, Q. H. Liu, R. Qin, J. Zhou, D. P. Yu, S. Nagase, W. N. Mei, Z. X. Gao and J. Lu, Tunable and sizable band gap of single-layer graphene sandwiched between hexagonal boron nitride, *NPG Asia Mater.*, 2012, **4**, 6.

27 Z. Y. Huang, X. Qi, H. Yang, C. Y. He, X. L. Wei, X. Y. Peng and J. X. Zhong, Band-gap engineering of the h-BN/MoS_2/h-BN sandwich heterostructure under an external electric field, *J. Phys. D: Appl. Phys.*, 2015, **48**, 205302.

28 G. A. Gelves, B. Lin, U. Sundararaj and J. A. Haber, Low Electrical Percolation Threshold of Silver and Copper Nanowires in Polystyrene Composites, *Adv. Funct. Mater.*, 2006, **16**, 2423–2430.

29 J. P. Perdew, K. Burke and M. Ernzerhof, Perdew, Burke, and Ernzerhof Reply, *Phys. Rev. Lett.*, 1998, **80**, 891.

30 S. Grimme, Semiempirical GGA-type density functional constructed with a long-range dispersion correction, *J. Comput. Chem.*, 2006, **27**, 1787–1789.

31 Y. C. Cheng, Z. Y. Zhu, Y. Han, Z. Y. Liu, B. C. Yang, A. Nie, W. Huang, R. Shahbazian-Yassar and F. Mashayek, Sodium-Induced Reordering of Atomic Stacks in Black Phosphorus, *Chem. Mater.*, 2017, **29**, 1350–1356.

32 Y. C. Cheng, Z. Y. Zhu and U. Schwingenschlogl, Cl-intercalated graphene on SiC: Influence of van der Waals forces, *EPL*, 2013, **101**, 27008.
33 M. D. Segall, P. J. D. Lindan, M. J. Probert, C. J. Pichard, P. J. Hasnip, S. J. Clark and M. C. Payne, *J. Phys.: Condens. Matter*, 2002, **14**, 2717–2744.
34 J. Heyd and G. E. Scuseria, Efficient hybrid density functional calculations in solids: Assessment of the Heyd–Scuseria–Ernzerhof screened Coulomb hybrid functional, *J. Chem. Phys.*, 2004, **121**, 1187–1192.
35 J. Heyd, G. E. Scuseria and M. Ernzerhof, Hybrid functionals based on a screened Coulomb potential, *J. Chem. Phys.*, 2003, **118**, 8207–8215.
36 P. J. Stephens, F. J. Devlin, C. F. Chabalowski and M. J. Frisch, AB-intio calculation of vibrational absorption and circular-dichroism spectra using density-function force-fields, *J. Phys. Chem.*, 1994, **98**, 11623–11627.
37 A. D. Becke, Density-functional thermochemistry. III. The role of exact exchange, *J. Chem. Phys.*, 1993, **98**, 5648–5652.
38 L. Dong, S. K. Yadav, R. Ramprasad and S. P. Alpay, Band gap tuning in GaN through equibiaxial in-plane strains, *Appl. Phys. Lett.*, 2010, **96**, 202106.
39 M. X. Xiao, T. Z. Yao, Z. M. Ao, P. Wei, D. H. Wang and H. Y. Song, Tuning electronic and magnetic properties of GaN nanosheets by surface modifications and nanosheet thickness, *Phys. Chem. Chem. Phys.*, 2015, **17**, 8692–8698.
40 Y. C. Cheng, Z. Y. Zhu, G. S. Huang and U. Schwingenschlogl, Grüneisen parameter of the G mode of strained monolayer graphene, *Phys. Rev. B: Condens. Matter Mater. Phys.*, 2011, **83**, 115449.
41 R. S. Jacobsen, K. N. Andersen, P. I. Borel, J. F. Pedersen, L. H. Frandsen, O. Hansen, M. Kristensen, A. V. Lavrinenkol, G. Moulin, H. Y. Ou, C. Peucheret, B. Zsigri and A. Bjarklev, Strained silicon as a new electro-optic material, *Nature*, 2006, **441**, 199–202.
42 R. X. Fei and L. Yang, Strain-Engineering the Anisotropic Electrical Conductance of Few-Layer Black Phosphorus, *Nano Lett.*, 2014, **14**, 2884–2889.
43 S. L. Zhang, Z. Yan, Y. F. Li, Z. F. Chen and H. B. Zeng, Atomically Thin Arsenene and Antimonene: Semimetal-Semiconductor and Indirect-Direct Band-Gap Transitions, *Angew. Chem., Int. Ed.*, 2015, **54**, 3112–3115.
44 G. Gui, J. Li and J. X. Zhong, Band structure engineering of graphene by strain: First-principles calculations, *Phys. Rev. B: Condens. Matter Mater. Phys.*, 2008, **78**, 075435.